Probing the microscopic nuclear matter self-organization processes in the neutron star crust

F. Sébille, V. de la Mota, and S. Figerou
SUBATECH, Ecole des Mines, Université de Nantes, CNRS/IN2P3, Nantes, France
(Received 27 July 2011; published 14 November 2011)

We investigate microscopic self-organization processes of nuclear matter in the outermost layers of neutron star crusts with the DYWAN model. In this framework a pure mean-field description of nuclear dynamics has been performed. Starting from initial crystalline lattices, which are expected in the most external regions, the system organizes itself in exotic structures. The present work focuses on the effects of both the initial lattice symmetries and the nuclear species on the morphology and on the evolution of those structures. The response of the system is analyzed when it is subjected to random fluctuations of the initial lattice.

DOI: 10.1103/PhysRevC.84.055801 PACS number(s): 26.60.Gj, 24.10.Cn

I. INTRODUCTION

Neutron stars (NSs) are cold and extremely compact objects, with temperatures $T \ll 1$ MeV and densities ranging from a few grams per cubic centimeter at the surface to 10^{15} g cm^{-3} at the center. As predicted in the early 1980s [1,2], and endorsed by recent works, nuclei may adopt exotic shapes at subnuclear densities. Ever since then these structures had concentrated the interest of many theoretical works [3–6]. They are supposed to be built as the consequence of the interplay between Coulomb and nuclear forces and to be sensitive to the equation of state (EOS) of nuclear matter. It has been argued that their existence may have important astrophysical consequences on macroscopic characteristics such as masses and radii [7], as well as on the cooling processes [8] of the star. In particular, their presence should affect the neutrino opacity [9] and the transport properties [10] of the crust.

We have recently developed a self-consistent dynamical model [11] in which nonspherical shapes are shown to appear as a consequence of nuclear microdynamics. The different structural phases involve low-energy excitations. We were interested in the dynamical exploration of those multiple low-lying energy configurations through a mean-field description in which residual interactions have been neglected. In our first calculations we have solved time dependent Hartree-Fock (TDHF)-like equations of motion for the one-body density matrix at zero temperature. In order to disentangle numerical from physical fluctuations, the first step was to check the corresponding numerical accuracy. The simulation has been shown to be extremely well conditioned, conserving metastable configurations during time intervals of several thousands of femtometers/c. On the other hand, isospin-dependent effective forces have been utilized for the treatment of the mean field and the sensitivity of the above structures to nuclear matter EOS was analyzed. These preliminary calculations have been performed on oxygen lattices built with simple cubic primitive cells. The occurrence of nuclei with exotic shapes such as rods, slabs, and other complex structures was observed and interpreted in terms of the effective force.

In this work we would like to complete our previous investigations of the NS crust matter in the framework of the present mean-field approach. The corresponding extension of the model beyond the mean-field description will be the aim of a forthcoming paper. Our interest relies on the self-organization of the nuclear matter from the lattice structures expected in the outer crust to either exotic structures or disordered patterns in the inner crust. Dynamical investigations are well suited to analyze such complex context, and therefore in order to contrast our results with other recent works we apply a criterion allowing us to compare the characterization of structures stemming from our model and from a molecular dynamical description [4].

Since in our preliminary calculations we have considered for simplicity only light nuclei lattices with simple cubic primitive cells, the purpose of this work is to make use of other initial arrangements of matter including heavier nuclei, in order to study the influence of various lattice symmetries and to study their corresponding behavior with the launching of random lattice perturbations.

This work is organized in the following way. In Sec. II we recall the bases of the model. In Sec. III a comparative analysis between two different definitions of structures is presented. Section IV is dedicated to the study of lattice perturbations in a simple cubic-type oxygen lattice for two isotopic composition. In Sec. V face-centered and body-centered cubic cells are considered. The consequence of the new lattice symmetries in the dynamics is investigated. Section VI is devoted to the study of iron lattices in order to analyze the impact of nuclear species. Conclusions are given in Sec. VII.

II. SURVEY OF THE MODEL

In this section we will restrict ourselves to an overview of the principal ingredients of our model, a detailed description of which can be found in Ref. [11]. In the range of temperatures and densities characteristic of the NS crust, the stellar matter is usually described in terms of a system of interacting nucleons in a uniform background of electrons. In order to address the microphysics of this region of the star we have developed a dynamical model in the spirit of the DYWAN model of nuclear collisions [12], built on the basis of projection methods (PMs) [13] and on mathematical wavelet theory [15].

From the Liouville–von Neumann equation of motion for the complete N-body density matrix, the PMs permit us to extract the equations of motion of relevant variables, which are coupled to the dynamics of irrelevant ones. In the case where the relevant variables are one-body observables it has

been shown [13,14] that the one-body density matrix ρ evolves according with the following equation:

$$i\hbar\dot{\rho} = [\mathcal{H}(\rho), \rho] + I(\rho), \tag{1}$$

where $\mathcal{H}(\rho)$ is the self-consistent Hamiltonian and $I(\rho)$ is the collision term. In the weak-coupling limit and in the Markovian approximation this collision term is the quantum version of the Boltzmann collision term for the Fermi-Dirac statistics. This equation belongs to the class of extended TDHF equations (ETDHF) that have been derived alternatively through other techniques such as the truncation of the quantum Bogoliubov-Born-Green-Kirkwood-Yvon (BBGKY) hierarchy for density matrices [16] or that of the Martin-Schwinger hierarchy for Green functions [17]. The introduction of multiparticle correlations will allow to go beyond this description. Nevertheless, in this work we remain at the lowest level of the description by neglecting the collision term under the condition that the intrinsic excitation of nuclei is almost vanishing and their dynamics is governed by the mean field. In order to be able to go efficiently beyond the mean-field approximation, and since the previously referred to theories encompass the correlation effects from a perturbative point of view, one purpose is also to stringently control and analyze the main contribution to the dynamics, i.e., the mean field. Equation (1) with $I(\rho) = 0$ is solved on a three-dimensional lattice satisfying periodic boundary conditions. The so-called supercell is built up with primitive cells, which, in general, differ from Wigner-Seitz (WS) cells. The implemented primitive cells are simple cubic (SC), face-entered cubic (FCC), and body-entered cubic (BCC) cells. In the initial condition a nucleus is prepared in an elementary cell either in its ground state or in excited states, according to mechanical or thermal constraints, by means of a static self-consistent procedure. The resulting single-particle (SP) wave functions are spanned in a basis of wavelets $|\alpha_i^\lambda\rangle$ [15], the subscript referring to the ith basis element of the one-body level λ. These last functions have interesting properties as defined symmetries, compact support and orthogonality, and can be approximated by simple analytical forms. At the same time, they provide strongly compressed representations of the system with an accurate description of the SP wave functions.

The N-body density matrix is then constructed with Slater determinants of SP wave functions. Its projection on the one-body space of states gives the corresponding one-body density matrix, which can be expressed as

$$\rho = \sum_{\lambda=0}^{N} \sum_{i,j} \beta_{i,j}^{\lambda} |\alpha_i^\lambda\rangle\langle\alpha_j^\lambda|, \tag{2}$$

where the parameters $\beta_{i,j}^{\lambda}$ are coefficients related to SP wave function decomposition in terms of wavelets. Owing to this decomposition the one-body density matrix is a function of a set of time-dependent correlated coordinates $\{\vec{\xi}(t), \vec{\chi}(t), \vec{\pi}(t), \vec{\phi}(t)\}$ corresponding to the first and second moments in coordinate and momentum spaces, respectively. The equations of motion of these quantities have been obtained from a variational principle [11]. They constitute a system of coupled nonlinear differential equations in terms of the wavelet transform of the effective nuclear potential $\mathcal{V} = \langle\alpha|V_q^{\mathrm{HF}}|\alpha\rangle$.

In this work we have chosen, for both the static and the dynamic calculations, a density-dependent zero-range effective interaction, with the following self-consistent field [11]:

$$V_q^{\mathrm{HF}}(\rho,\xi) = \frac{t_0}{\rho_\infty}\rho + \frac{t_3}{\rho_\infty^{\nu+1}}\rho^{\nu+1} + \frac{c}{{\rho_\infty}^2}\xi^2 + \frac{4qc}{{\rho_\infty}^2}\rho\xi + \frac{\Omega}{3{\rho_\infty}^2}\xi^2 + \frac{4q\Omega}{3{\rho_\infty}^2}(\rho-\rho_\infty)\xi + V_q^C, \tag{3}$$

where ρ_n and ρ_p stand for neutron and proton densities, $\rho = \rho_n + \rho_p$, $\xi = \rho_n - \rho_p$, and $q = 1/2$ for neutrons and $-1/2$ for protons, $\rho_\infty = 0.145$ fm^{-3} is the saturation density of infinite nuclear matter, and V_q^C is the Coulomb potential. The standard values of the parameters are

$$\nu = 1/6, \quad t_0/\rho_\infty = -356 \text{ MeV fm}^3$$
$$t_3/\rho_\infty^{\nu+1} = 303 \text{ MeV fm}^{3(\nu+1)}.$$

We have chosen $c = 20$ MeV and $\Omega = -100$ MeV in order to reproduce the typical values of baryon density energies in infinite matter as well as the principal static characteristics of nuclei, as binding energies, radii, and equilibrium densities. The parameters c and Ω are related to the familiar symmetry coefficients J and L [11]. The current values fall in with typical values in macroscopic and microscopic calculations [18]. The Coulomb term for protons is calculated using Ewald summation techniques [19], adapted to the calculation of long-range potentials in periodic systems. It consists basically in recasting V^C into two convenient terms, each of which can be calculated in a fast and efficient way. The current values of the parameters of Eq. (3) will not be changed in the present work.

III. REFERENCE THRESHOLD DENSITY

One of the salient results of Ref. [11] is the appearance of nonspherical structures, and the transitions between them, as a consequence of the self-consistent dynamical evolution. As mentioned in Sec. II, density matrices are built from Slater determinants of SP wave functions providing time-dependent continuous local densities in configuration space. The various morphological structures are characterized by the average density $\langle\rho\rangle$ and the threshold density ρ_t. The former is the number of particles inside the supercell divided by the related volume, the choice of which allows us to explore diverse configurations with neighboring energies. The latter determines domains in the three-dimensional space where the nuclear density distribution is constrained by the condition $\rho(\vec{r}) \geqslant \rho_t$. Each density threshold gives a set of boundary regions of equal density (isosurfaces) corresponding to well-defined morphological structures. Due to the spreading of the wave functions the density distribution is inhomogeneous and different density threshold values lead to various shapes, similarly to the variation of coastal contours with tidal movements. In this way at a given time the spatial density distribution is unique but the isosurfaces, i.e., the morphological structures, are not since they depend on the choice of the threshold density. In addition to dripped neutrons, low-density regions linking different clusters are built as a result of the spreading of nucleon wave functions. These regions experience densities lower than the saturation value of nuclear matter and, accordingly, they are revealed only

at low values of ρ_t. In Ref. [11] it has been stressed that these structures are in general intermingled, rendering difficult their characterization. In the above reference, phase structure diagrams have been built in the $(\rho_t, \langle\rho\rangle)$ plane for a variety of systems with distinct isotopic composition. Due to their dynamical origin, the corresponding shapes in phase diagrams are the result of an averaging procedure over different times, the consequence being a diagram pattern exhibiting some small fluctuations around a smooth behavior which could be obtained by smearing over a greater number of times.

Most models deal with one-dimensional phase representations as a function of the mean density [1–4], associating a unique morphological structure to a given average density. In our context, i.e., in the $(\rho_t, \langle\rho\rangle)$ plane, this means that a choice of a threshold density of reference $\rho_t^{\rm ref}$ must be made in order to compare with other approaches. To this end various criteria may be applied. In Ref. [4] a threshold density has been derived from the following condition:

$$\left(\frac{d^2(\mathcal{V}/\mathcal{A})}{d\rho_t^2}\right)_{\rho_t^{\rm ref}} = 0, \tag{4}$$

where $\mathcal{V}$ and $\mathcal{A}$ are the volume and the surface area, respectively, corresponding to the regions where the local density is $\rho(\vec{r}) \geqslant \rho_t$. In our model both quantities, $\mathcal{V}$ and $\mathcal{A}$, have been calculated using morphological image analysis (MIA) techniques [20].

As mentioned in Ref. [4] condition (4) is not always suitable and often it is not possible to extract a threshold density of reference $\rho_t^{\rm ref}$ due to the diffuseness of the density distribution entailed either by nonzero temperatures or by the wave function spreadings. In the following, aiming at working out a significant comparison, we address only those situations in which $\rho_t^{\rm ref}$ can be unambiguously extracted.

In Fig. 1 are plotted the neutron phase diagrams corresponding to SC lattices of oxygen isotopes for two distinct values of the proton fraction, x_p= 0.5 in part (a) and 0.2 in part (b).

In these pictures the distribution of different shapes (spherical, cylindrical, planar slab, spongelike, and bubble-like) is given in terms of ρ_t and of the average density normalized to the saturation value $\langle\rho\rangle/\rho_\infty$. The threshold density $\rho_t^{\rm ref}$ resulting from Eq. (4) is shown by full squares, the widths of which are equal to their corresponding numerical uncertainties.

In these cases the calculated reference values are roughly independent of the mean density. They are located around 0.05 to 0.06 fm^{-3} at $x_p = 0.2$ and fall under 0.04 fm^{-3} at the proton fraction $x_p = 0.5$. In both plots of Fig. 1, following the corresponding $\rho_t^{\rm ref}$ values, one retrieves globally the same phase sorting in terms of $\langle\rho\rangle$ as in one-dimensional phase diagrams [4]. By considering for instance cold matter diagrams at $x_p = 0.5$ and 0.3 in Fig. 3 of Ref. [4], the same structures appear at roughly the same values of the average densities. Some differences may nevertheless appear, as in the case of symmetric nuclear matter for which slablike structures are not present in the actual description [Fig. 1(a)]. This is a consequence of the underlying mean-field evolution where no perturbations nor dissipation have been implemented. The resulting dynamics preserves strictly the symmetries of the initial conditions, which in this particular case are such that

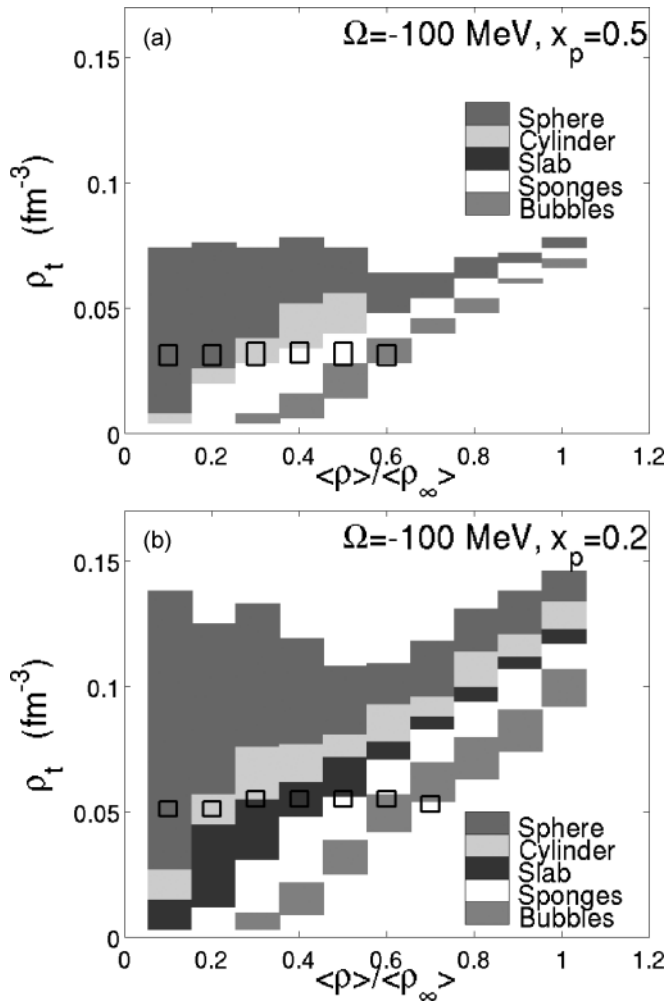

FIG. 1. Neutron structure distributions as a function of the threshold density ρ_t and of the normalized neutron mean density $\langle\rho\rangle/\rho_\infty$ for two proton fractions $x_p = 0.5$ (a) and $x_p = 0.2$ (b).

planar structures are not favored. It must be pointed out that the occurrence of these structures in Ref. [4] is concentrated only in a narrow density region around $0.35\rho_\infty$.

IV. EFFECTS OF LATTICE PERTURBATIONS

As already stated, a stringent mean-field treatment should preserve the initial symmetries; consequently, the stability of the corresponding solutions against numerical fluctuations has been checked. Indeed, in Ref. [11] it has been shown that the initial lattice symmetries are preserved during the evolution of the system over several thousands of femtometers/c. Starting from a low-lying energy nonequilibrium initial state, the system passes through different structural configurations which are energetically equivalent. In principle, a variety of initial conditions can be considered. In our previous works SC lattices with slightly deformed oxygen isotopes, with proton fractions 0.1, 0.2, and 0.5, have been employed to build the initial state. It is well known in condensed matter physics that SC lattices are not the most stable ones with respect to the Coulomb interaction. In theses cases mean-field treatments

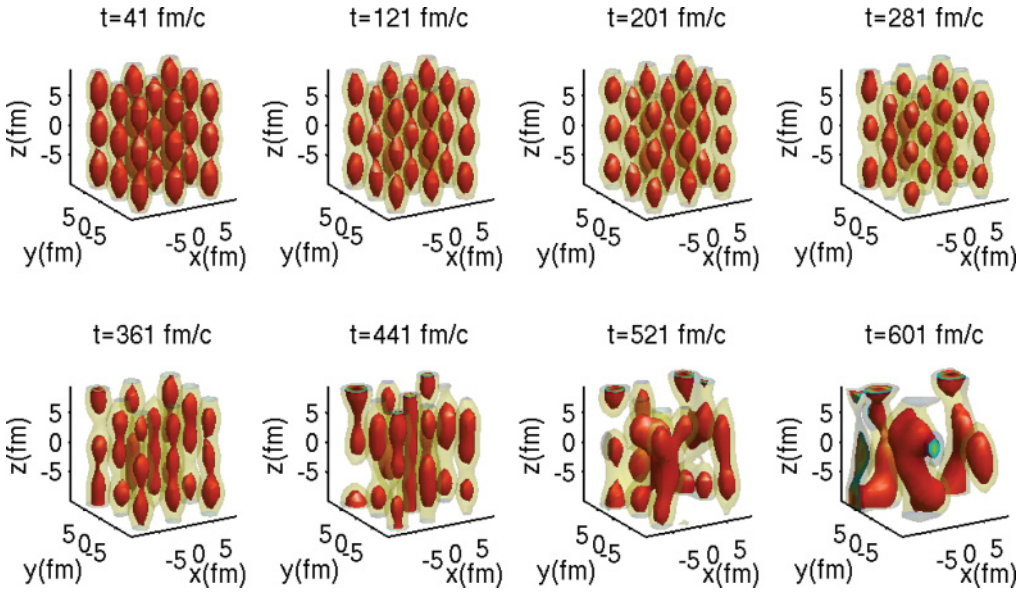

FIG. 2. (Color online) Neutron density time evolution of a perturbed simple cubic lattice of oxygen isotopes with proton fraction $x_p = 0.5$, mean density $\langle\rho\rangle = 0.4\rho_\infty$, and threshold density $\rho_t = 0.04$ fm^{-3}.

lead to various metastable states for which the introduction of small perturbations is susceptible to provoke the breaking of the initial symmetries.

As underlined by other authors [21] the inner crust of a neutron star is an extremely complex system in which the appearance of disordered phases could be favored. There is a special interest in investigating how nuclear matter, for a given proton fraction, self-organizes dynamically under the influence of the equation of state. In order to study the feasibility of those disordered phases, perturbations of the initial arrangements built in previous works have been introduced and their influence on the overall dynamics has been analyzed. To this end we considered SC lattices of oxygen isotopes, with $x_p = 0.2$ and 0.5, the positions of which have been slightly shifted at random from the lattice sites at the initial time.

The time evolution of the supercell density is represented in Figs. 2 and 3 in the cases where the average density is $\langle\rho\rangle = 0.4\rho_\infty$ and the proton fractions are $x_p = 0.5$ and 0.2, respectively. These shape sequences have been obtained, respectively, with the threshold densities $\rho_t = 0.04$ and $\rho_t = 0.05$.

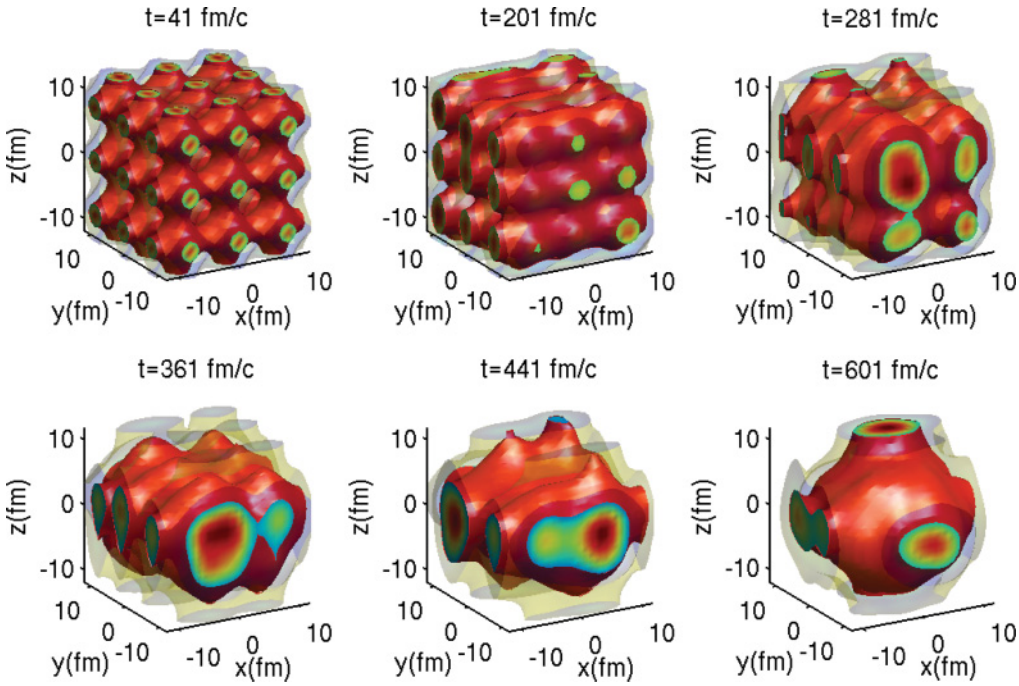

FIG. 3. (Color online) Same as Fig. 2 with proton fraction $x_p = 0.2$.

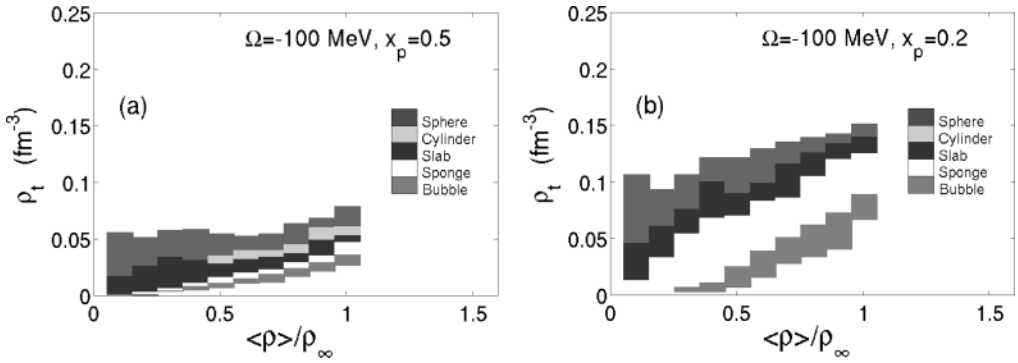

FIG. 4. Neutron phase diagrams of perturbed simple cubic lattices of oxygen isotopes with proton fractions $x_p = 0.5$ (a) and $x_p = 0.2$ (b).

A gradual loss of the initial arrangement of nuclei is observed in both pictures. From an ordered array of regular deformed nuclei the system evolves toward a heterogeneous configuration of clusters with different masses and shapes. The small initial perturbations then generate sufficiently strong density fluctuations so as to provoke a rearrangement of matter molding heavy aggregates. A salient difference between the two dynamics is the fact that isospin-asymmetric nuclei tend to collapse into one large cluster occupying the whole supercell, in contrast to the isospin-symmetric case in which matter is mainly composed of small or intermediate mass clusters. The fact that a lowering in the proton fraction generates a single aggregate in the supercell (or, equivalently, an infinite one taking periodic conditions into account) can be interpreted as a consequence of the increase in neutron wave functions diffusivity. Indeed, as the proton fraction decreases, the number of dripped neutron increases and the nucleons become more delocalized with significant overlap in configuration space. Therefore the local competition between nuclear and Coulomb interactions covers broader regions in the three-dimensional space.

As stated before, structural phase diagrams allow us to understand the occurrence of the different embedded structures which appear for a given value of mean density as a function of the threshold density. In perturbed lattices some amount of energy is initially stocked in cluster collective modes, providing us with the opportunity to explore the energy minima manifold corresponding to the various density distributions. Since mixed phases can appear simultaneously only the most frequent structure is associated with a given value of the threshold density for constructing the two-dimensional structure diagram.

Figure 4 shows the phase diagrams corresponding to the neutronic population of the perturbed oxygen lattice with proton fractions $x_p = 0.5$ (a) and $x_p = 0.2$ (b). While in the nonperturbed case slab structures were lacking, we observe here that the inclusion of perturbations induces the formation of planar structures and the disappearance of rodlike structures in the case of the lowest protonic fraction. In this case spongelike structures, which are a consequence of SP wave function delocalization, are preponderant and contribute to partially preserve the initial symmetries despite the strong reorganization of matter inside the supercell.

V. INFLUENCE OF LATTICE SYMMETRIES

In the previous calculations SC primitive cells have been utilized to construct the initial lattice due to their simplicity. The next step was to implement other three-dimensional crystal lattices displaying new symmetries and to analyze their influence on the morphologic properties of the system. The FCC primitive cell is represented in Fig. 5.

In this arrangement, the nuclei which are located at the vertices of the cube contribute with a weight of $1/8$ and those in the center of the faces contribute with $1/2$, the number of nuclei being therefore equal to 4.

The time evolution of the supercell density is represented in Fig. 6 in the case in which it is composed of individual FCC cells of oxygen isotopes with proton fraction $x_p = 0.5$. The average density in the supercell is $0.4\rho_\infty$ and the threshold density is $\rho_t = 0.04$. The system has been initially perturbed in the same way as in Sec. IV. Comparing the structures of Fig. 6 with those of the SC case in Fig. 2, at equal times, we see that the symmetry of the new initial condition modifies the corresponding density evolution. Indeed, despite the random perturbations imposed on the nuclei positions, the system attempts to preserve symmetries exhibiting stringy or cylindrical structures. At sufficiently long times, the dominant arrangement at the supercell level is a single rodlike structure.

The corresponding phase diagram has been plotted in Fig. 7(a), where the presence of cylindrical structures is shown to be dominant for average densities higher than about $0.3\rho_\infty$. By lowering the threshold density and making the bins narrower, other structures such as slabs and bubbles are also present. The nonuniformity of the density distribution is also evidenced at higher density thresholds where the structure diagram displays spherical-like structures.

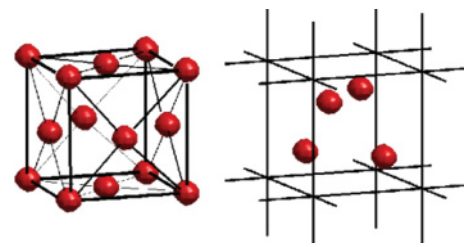

FIG. 5. (Color online) Left: Schematic representation of an FCC lattice. Right: An FCC primitive cell with four nuclei.

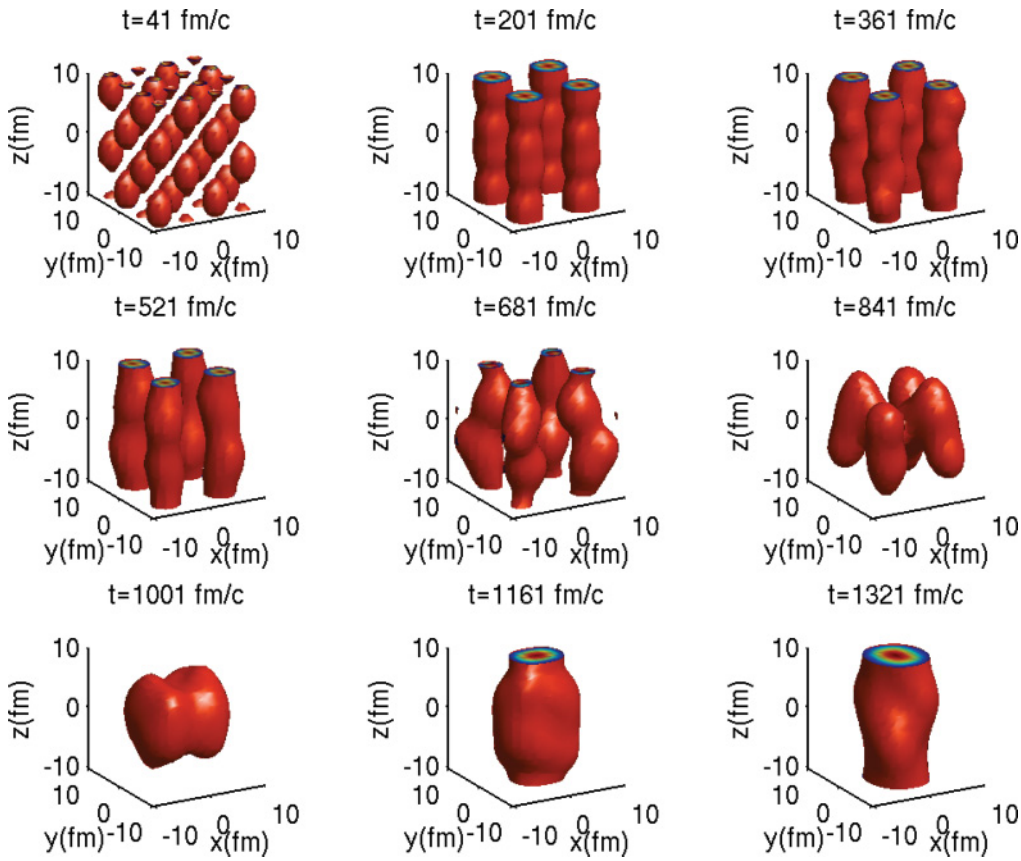

FIG. 6. (Color online) Density profiles of a perturbed supercell of 0.5 proton fraction oxygen isotopes in FCC lattices. The mean and threshold densities are $\langle\rho\rangle = 0.4\rho_\infty$ and 0.04 fm^{-3}, respectively.

In Fig. 7(b) we have represented the diagram corresponding to the proton fraction $x_p = 0.2$. In this case rods are nearly missing, the dominant structures are spherical at low mean densities, and, as this quantity increases, the system undergoes a smooth transition toward more homogeneous density distributions, the structures appearing only at higher ρ_t. This fact can be seen as a consequence of the growth of the number of dripped neutrons with the average density. Since these neutrons are delocalized the corresponding wave functions are wider and their contribution to the local density tends to fill up the entire space. This clearly different behavior between the two isospin asymmetries for the FCC lattice is not observed in the SC case in Fig. 4.

The same kind of analyses have been performed with the BCC unit cell, a schematic representation of which is given in Fig. 8. In this arrangement there are two nuclei per unit cell: one of them is located on the center and has a weight of 1, and the others are placed at the eight corners, their corresponding weights being 1/8.

In Fig. 9 we have plotted the time evolution of the spatial density distribution in a perturbed BCC oxygen lattice with proton fraction 0.5. The system evolves to a heavy cluster in

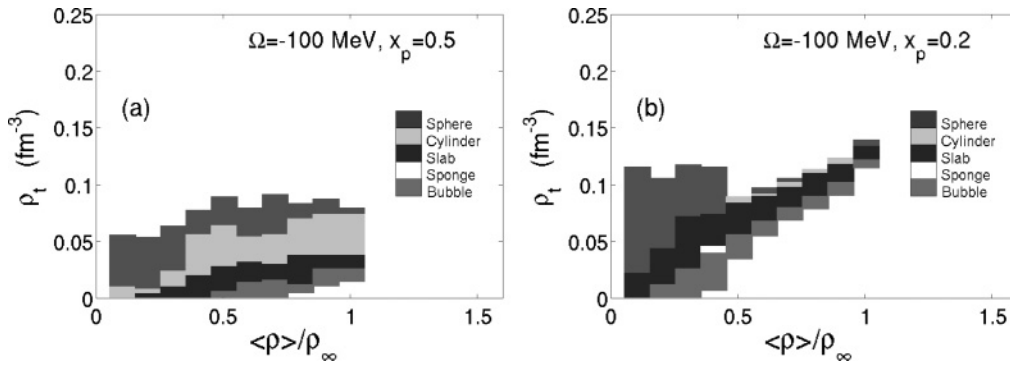

FIG. 7. Neutron phase diagrams of perturbed FCC lattices of oxygen isotopes with proton fractions $x_p = 0.5$ (a) and $x_p = 0.2$ (b).

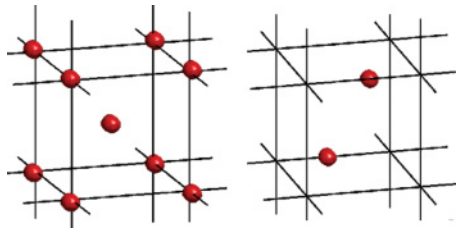

FIG. 8. (Color online) Left: Schematic representation of a BCC cell. Right: Representation of two translated nuclei in the same cell.

which the initial symmetries have been washed out. Comparing the temporal evolutions of the three different configurations (Figs. 2, 7, and 9) we see that the one corresponding to the FCC cell arrangement is clearly the more stable in the sense that matter remains in organized rodlike shapes for longer times. These results evidence the stability of nonequilibrium structures in FCC arrangements (Fig. 6) against SC or BCC configurations for the same mean density.

This assertion goes along with the usual behavior of atomic lattices in condensed matter approaches. A well-known result in this field is the instability of SC lattices with central forces. The situation is analogous in our description in the cases in which the average densities are low. In that cases the nuclear field between clusters, initially located in lattice sites, is negligible. This is a conclusive result which endorses the fact that the actual dynamical model is clearly sensitive to initial lattice symmetries.

In Fig. 10 are represented the structure diagrams for neutrons in the perturbed oxygen BCC lattice with proton fractions $x_p = 0.5$ (a) and $x_p = 0.2$ (b).

The difference between the various lattice behaviors is clearly emphasized in the asymmetric $x_p = 0.2$ case, with the appearance of larger regions with a homogeneous density distribution beneath the bubble-like zone. These last structures correspond to the lower values of the threshold density. It can been easily seen that the area related to the homogeneous density strongly increases when one switches from an SC lattice to a BCC lattice and finally to an FCC one. This is in obvious relation with the packing factor of the concerned lattices, which grows, respectively, from 0.524 to 0.680 to 0.740.

VI. SENSITIVITY TO INITIAL NUCLEAR SPECIES

In order to investigate the influence of the charge and the mass of nuclear species on the onset and on the dynamical evolution of structures, iron nuclei with different isotopic compositions have been considered. In Fig. 11 the phase diagrams of SC iron lattices corresponding to proton fractions $x_p = 0.5$ (a) and to $x_p = 0.3$ (b) are shown in the case in which the initial state is not perturbed.

In both cases planar structures are mainly favored in a wide range of threshold densities for all mean densities, the broader contribution being in the case of asymmetric matter. A good part of these diagrams concerns also rods for both proton fractions at high threshold densities. On average, these structures are preserved during times of the order of thousands

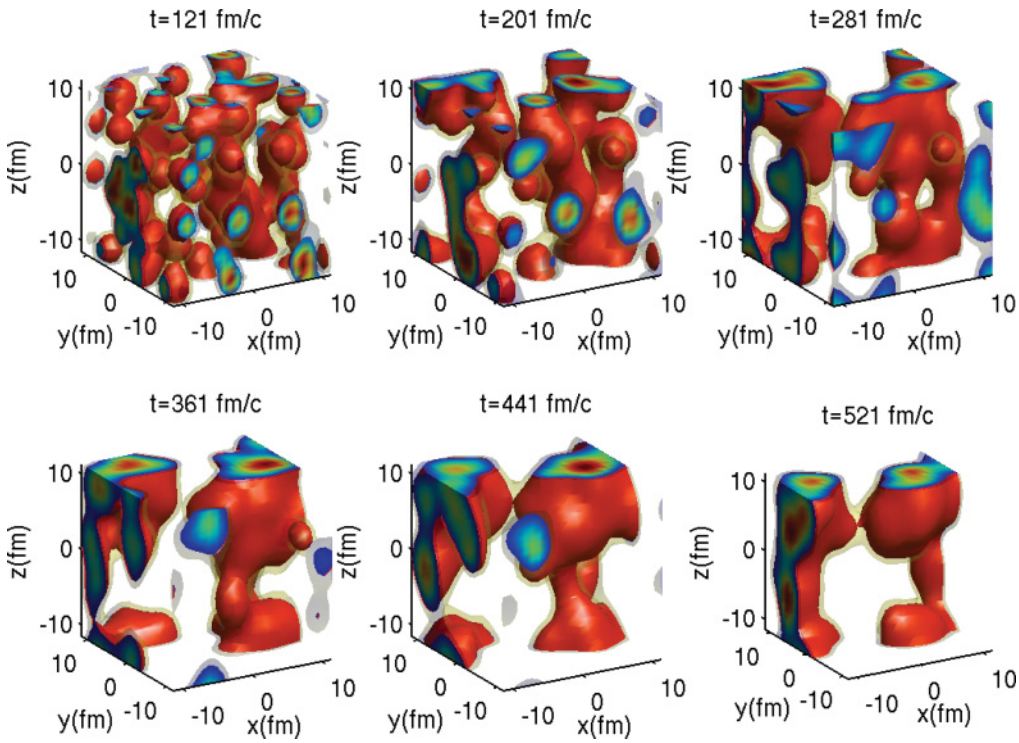

FIG. 9. (Color online) Density profiles of a perturbed supercell of 0.5 proton fraction oxygen isotopes in BCC lattices. The mean and threshold densities are $\langle\rho\rangle = 0.4\rho_\infty$ and 0.03 fm^{-3}, respectively.

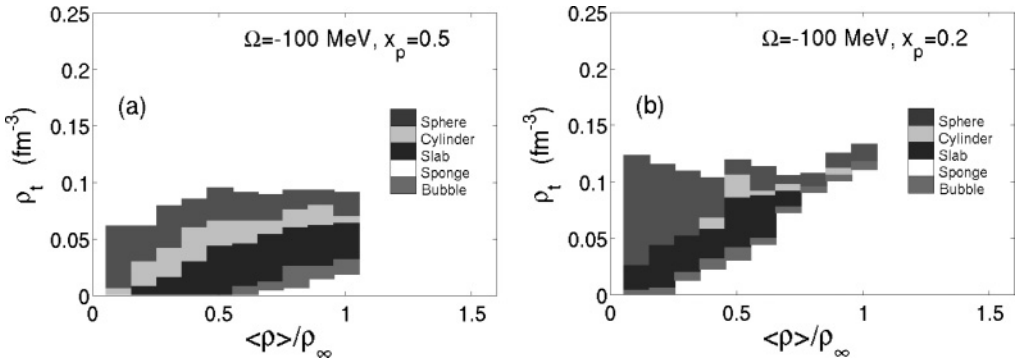

FIG. 10. Neutron phase diagrams of perturbed BCC lattices of oxygen isotopes with proton fractions $x_p = 0.5$ (a) and $x_p = 0.2$ (b).

of femtometers/c. They are a direct consequence of the initial lattice symmetries and of the anisotropic geometry of the iron nuclei, which is no longer spherical as were oxygen nuclei in the previous analysis.

The corresponding structure diagram can be conveniently compared for oxygen and iron lattices through, respectively, Figs. 11 and 1. In the latter, slablike shapes are present only over a narrow density domain in asymmetric nuclear matter and they are completely missing in the symmetric case. The dynamical appearance of slablike structures in Fig. 11 can be understood as the result of a subtle interplay between the strong attractive mean field created by the massive iron nuclei and the Coulomb interaction. The question of whether the observed steady behavior for the nonperturbed iron lattice is delayed or preserved in the presence of perturbations can be addressed.

The time evolution of the spatial density of iron nuclei in the symmetric $x_p = 0.5$ case is exhibited in Fig. 12 with two kinds of cells: SC in (a) and FCC in (b).

The overall mean density is $\langle\rho\rangle = 0.1\rho_\infty$ in panel (a) and $\langle\rho\rangle = 0.4\rho_\infty$ in panel (b), the threshold density being $\rho_t = 0.05$ fm^{-3} in both cases. In these calculations nuclei positions have been randomly shifted from the lattice sites at the initial time. The resulting structures for FCC cells are mostly planar and still conserve the fingerprints of the initial symmetries. The observed structures in the SC lattice are the deformed individual iron nuclei which undergo shape oscillations around their initial condition. The stability and symmetry of nonequilibrium structures in the iron lattice seem to not be substantially modified by perturbations, regardless of cell type. This behavior can be interpreted as a consequence of the relative weight of Coulomb and nuclear forces between neighboring nuclei. Actually, the magnitude of the random perturbations applied to both lattices are of the same order; nevertheless, the corresponding effects are different. For symmetric systems with the same average density, the long-range Coulomb potential scales with $(A_1/A_2)^{4/3}$, A_i being the masses of nucleus i (here namely either the oxygen nucleus or the iron nucleus), while the short-range nuclear potential between nearest neighbors at low densities is weaker. Comparatively, the Coulomb force strength involved in the heaviest lattice is stronger than for the lighter one and dominates the dynamics. On the other side, due to the distances between nuclear sites in both systems, a small perturbation on the iron lattice does not affect the dominant character of the Coulomb force, whereas for the oxygen lattice the random displacements can make neighboring nuclei sufficiently near to feel the effects of the corresponding potential wells. This can explain why with the onset of perturbations the initial oxygen-like species evolves into a wide variety of exotic shapes or even toward amorphous matter, while in the iron lattice the matter self-organizes, exploring a restricted set of structures.

It is worthwhile to emphasize that the different behaviors described here related to the two kinds of nuclear species placed initially on the lattice sites agree with the trend pointed out in thermodynamical [22] and in linearized Vlasov

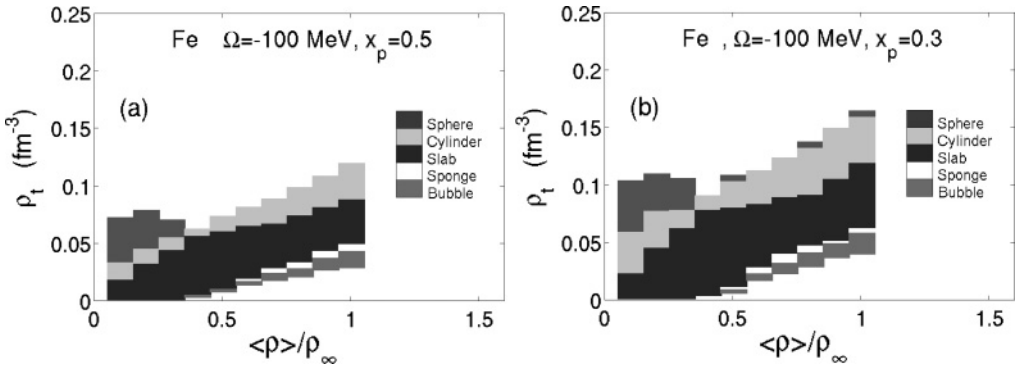

FIG. 11. Neutron phase diagrams of nonperturbed iron isotopes with proton fractions $x_p = 0.5$ (a) and $x_p = 0.3$ (b) in simple cubic cell lattices.

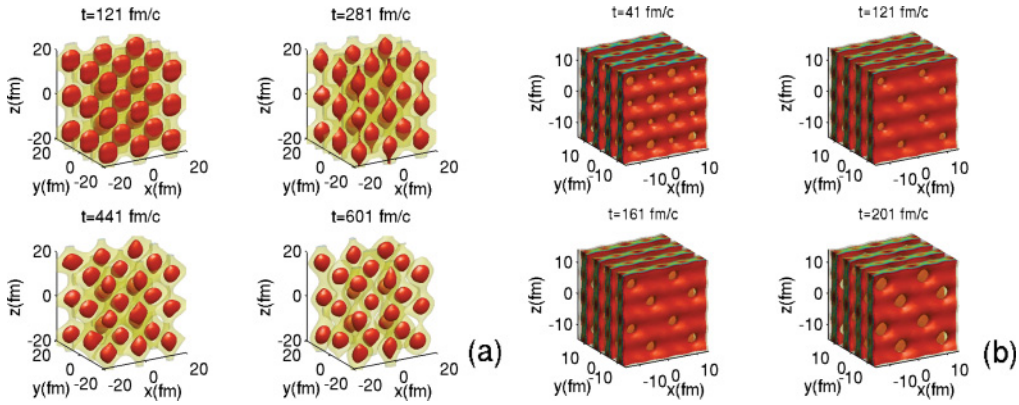

FIG. 12. (Color online) Density profiles of perturbed iron lattices with 0.5 proton fraction using simple cubic [face-centered] cells (a) [(b)]. The mean densities are $\langle\rho\rangle/\rho_\infty = 0.1$ in (a) and 0.4 in (b). The threshold density is 0.05 fm^{-3} in both cases.

dynamical approaches [23] with initial conditions provided by uniform distributions at subsaturation densities. It is mentioned that the treatment of the Coulomb interaction in a globally neutral system, under the assumption of a uniform distribution of electrons, induces a rigidity in the system which tends to inhibit the onset of instabilities and symmetry breaking.

VII. CONCLUSIONS

The microscopic DYWAN model has been recently developed in order to investigate the nuclear dynamics in the outer layers of neutron stars. In this framework, the occurrence of self-organized structures in nuclear matter has been established [11] as well as the sensibility of their morphology to the equation of state.

In this work, we first introduced a comparative analysis with other approaches [4] which investigate the possible morphological structures experienced in the crust through a one-dimensional phase representation of the structure sorting in terms of the average density. An equivalence between the corresponding criteria for the structure recognition was emphasized. Provided that the density of the system is constrained to satisfy geometrical conditions, the structural phase sorting is similar in both descriptions. Notwithstanding, in the DYWAN model the implemented effective interaction was different and the initial symmetries were fully conserved, in accordance with a pure mean-field study.

Pursuing our first investigations [11], we have analyzed the response of those structures to a variation of the initial conditions in order to understand the relationship of our results to various aspects such as lattice symmetries, symmetry breaking, and nuclear species.

The issue of initial symmetry breaking is addressed as follows: The positions of the nuclei have been slightly shifted at random from the SC lattice sites for oxygen nuclei with different isotopic compositions. The effects of perturbations are to destroy the initial symmetries. Nevertheless, in the case of the low proton fraction $x_p = 0.2$ the initial lattice regularity is merely preserved. This fact is illustrated when the system aggregates in a single heavy cluster holding the overall supercell. Conversely, in the $x_p = 0.5$ case a variety of irregularly distributed intermediate-mass clusters are found. In addition, the corresponding phase diagrams in the ρ_t versus $\langle\rho\rangle$ plane reveals the occurrence of planar structures which were lacking in the nonperturbed isospin symmetric case.

We analyzed the importance of cell symmetry by implementing FCC and BCC lattices, in addition to the SC ones. In all cases the system was subjected to initial perturbations. In both FCC and BCC lattices the system evolves toward a single cluster per supercell. In the former case a nonequilibrium steady cylindrical structure is formed in symmetric systems. In the latter the initial symmetries are washed out. By lowering the proton fraction, the system enters into a uniform phase for a wide density domain.

Finally, the sensitivity to the nuclear mass composition has been considered by studying the evolution of a perturbed iron lattice in SCC and FCC configurations. In both cases the systems remain in a steady nonequilibrium state, which corresponds to planar or to deformed spherical shapes, depending on the choice of the threshold density value.

In the present version of the model, individual nucleons, either bound or unbound, evolve in a self-consistent mean field by holding in the entire supercell under periodic boundary conditions. The occurrence of heavy aggregates and uniform phases at low proton fraction is deeply related to the ability of the model to describe the spreading of wave functions widths corresponding to unbounded nucleons. Investigations of the energy landscape in inhomogeneous nuclear matter at subnuclear densities are the purpose of forthcoming investigations. Owing to the sensitivity of the system to the spatial organization, such that several shapes and geometries can exist at the same density in various areas of the star, refined energy evaluations of the different structural phases will be done, addressing specially the estimation of the liquid and shell-energy contributions, which are naturally contained in our self-consistent description. Nevertheless, the formation and transitions between these nonequilibrium structures can be strongly modified using more complex nonlocal effective forces [24] and going beyond a pure mean-field description. These investigations are currently in progress.

[1] D. G. Ravenhall, C. J. Pethick, and J. R. Wilson, Phys. Rev. Lett. **50**, 2066 (1983).

[2] M. Hashimoto, H. Seki, and M. Yamada, Prog. Theor. Phys. **71**, 320 (1984).

[3] K. Oyamatsu, Nucl. Phys. A **561**, 431 (1993); K. Oyamatsu and M. Yamada, *ibid.* **578**, 181 (1994); M. Onsi, A. K. Dutta, H. Chatri, S. Goriely, N. Chamel, and J. M. Pearson, Phys. Rev. C **77**, 065805 (2008); T. Maruyama, T. Tatsumi, D. N. Voskresensky, T. Tanigawa, and S. Chiba, *ibid.* **72**, 015802 (2005); T. Maruyama, T. Tatsumi, and S. Chiba, Nucl. Phys. A **834**, 561c (2010).

[4] G. Watanabe, K. Sato, K. Yasuoka, and T. Ebisuzaki, Phys. Rev. C **66**, 012801(R) (2002).

[5] G. Watanabe, K. Sato, K. Yasuoka, and T. Ebisuzaki, Phys. Rev. C **69**, 055805 (2004); H. Sonoda, G. Watanabe, K. Sato, T. Takiwaki, K. Yasuoka, and T. Ebisuzaki, *ibid.* **75**, 042801(R) (2007).

[6] P. Magierski, A. Bulgac, and P.-H. Heenen, Nucl. Phys. A **719**, 217c (2003); W. G. Newton and J. R. Stone, Phys. Rev. C **79**, 055801 (2009); P. Gogëlein, E. N. E. van Dalen, C. Fuchs, and H. Müther, *ibid.* **77**, 025802 (2008).

[7] G. Haensel, A. Y. Potekhin, and D. G. Yakovlev, *Neutron Stars 1: Equation of State and Structure* (Springer, New York, 2006).

[8] D. Page, U. Geppert, and F. Weber, Nucl. Phys. A **777**, 497 (2006); D. G. Yakovlev and C. J. Pethick, Annu. Rev. Astron. Astrophys. **42**, 169 (2004).

[9] C. J. Horowitz, M. A. Perez-Garcia, and J. Piekarewicz, Phys. Rev. C **69**, 045804 (2004); C. J. Horowitz, M. A. Perez-Garcia, J. Carriere, D. K. Berry, and J. Piekarewicz, *ibid.* **70**, 065806 (2004); A. Burrows, S. Reddy, and T. A. Thompson, Nucl. Phys. A **777**, 356 (2006); H. Sonoda, G. Watanabe, K. Sato, T. Takiwaki, K. Yasuoka, and T. Ebisuzaki, Phys. Rev. C **75**, 042801(R) (2007).

[10] C. J. Horowitz and D. K. Berry, Phys. Rev. C **78**, 035806 (2008).

[11] F. Sébille, S. Figerou and V. de la Mota, Phys. Nucl. A **822**, 51 (2009); F. Sébille, V. de la Mota, I. C. Sagrado Garcia, J. F. Lecolley and V. Blideanu, Phys. Rev. C **76**, 024603 (2007).

[12] B. Jouault, F. Sébille, and V. de la Mota, Nucl. Phys. A **628**, 119 (1998).

[13] R. Balian, Y. Alhassid, and H. Reinhardt, Phys. Rep. **131**, 1 (1986).

[14] H. Reinhardt, P.-G. Reinhard and K. Goeke, Phys. Lett. B **151**, 177 (1985).

[15] M. Unser and A. Aldroubi, in *Wavelets, Volume 2: A Tutorial in Theory and Applications (Wavelet Analysis and Its Applications)*, edited by C. K. Chui, (Academic, New York, 1992); I. Daubechies, *Ten Lectures on Wavelets* (American Mathematical Society, Providence, RI, 1992); S. Mallat, *A Wavelet Tour of Signal Processing* (Academic, New York, 1999).

[16] C. O. Dorso and E. S. Hernández, Phys. Rev. C **26**, 528 (1982); E. S. Hernández and V. de la Mota, J. Phys. G **13**, L189 (1987).

[17] C.-Y. Wong, H. H. K. Tang, Phys. Rev. C **20**, 1419 (1979).

[18] S. Yoshida and H. Sagawa, Phys. Rev. C **73**, 044320 (2006); K. Oyamatsu and K. Iida, *ibid.* **75**, 015801 (2007); B.-A. Li, L.-W. Chenb, and C. M. Koc, Phys. Rep. **464**, 113 (2008); M. Di Toro, V. Baran, M. Colonna, G. Ferini, T. Gaitanos, V. Giordano, V. Greco, L. Bo, M. Zielinska-Pfabe, S. Plumari, V. Prassa, C. Rizzo, J. Rizzo and H. H. Wolter, Prog. Part. Nucl. Phys. **62**, 389 (2009); V. Baran, M. Colonna, V. Greco, and M. Di Toro, Phys. Rep. **410**, 335 (2005).

[19] A. Y. Toukmaji and J. A. Board Jr., Comput. Phys. Commun. **95**, 73 (1996).

[20] K. Michielsen and H. De Raedt, Phys. Rep. **347**, 461 (2001).

[21] P. Magierski and P.-H. Heenen, Phys. Rev. C **65**, 045804 (2002).

[22] C. Ducoin, K. H. O. Hasnaoui, P. Napolitani, Ph. Chomaz, and F. Gulminelli, Phys. Rev. C **75**, 065805 (2007); C. Ducoin, Ph. Chomaz, and F. Gulminelli, Nucl. Phys. A **771**, 68 (2006).

[23] C. Providencia, L. Brito, S. S. Avancini, D. P. Menezes, and Ph. Chomaz, Phys. Rev. C **73**, 025805 (2006); H. Pais, A. Santos, L. Brito, and C. Providencia, *ibid.* **82**, 025801 (2010).

[24] D. T. Loan, N. H. Tan, and D. T. Khoa, and J. Margueron, Phys. Rev. C **83**, 065809 (2011); J. Margueron, E. van Dalen, and C. Fuchs, *ibid.* **76**, 034309 (2007); F. Chappert, M. Girod, and S. Hilaire, Phys. Lett. B **668**, 420 (2008).